

General Coupling Method for Stripline Ferrite Circulators: Application on Dual-Band Devices With Complex Central Conductor Shape

Vincent Olivier¹, Thierry Monediere, Bertrand Lenoir¹, Hamza Turki¹, Christophe Breuil, Philippe Pouliguen¹, *Member, IEEE*, and Laure Huitema¹, *Member, IEEE*

Abstract—This article presents two original, efficient, and rigorous methodologies for coupling ferrite circulators of complex shapes. Indeed, by using a central conductor of any shape or geometry, an optimized circulation phenomenon can be achieved because of both methods. This article details and analyzes the two methods developed. They will be validated by the measurement of a stripline circulator with a triangular central conductor operating around 8 GHz. At the end of this first study, one of the two methods will be selected and implemented in a more complex case since we will adapt it to a dual-band operation.

Index Terms—Circulator design, complex shape, dual band, ferrite, Y-junction circulators.

I. INTRODUCTION

FERRITE circulators are microwave nonreciprocal passive components. Their nonreciprocity is due to the presence in their structure of magnetized ferrite materials. These devices have been the topic of many studies, which have led to numerous innovations, such as broadband [1], [2], self-biased [3]–[5], multifunction [6], [7], 3-D printed [8], or multiband [9]–[11] circulators. Fig. 1 shows the classical geometry of a stripline circulator, which is made of two magnetized ferrite disks separated by a central conductor. Three access lines [Fig. 1(b)] separated from each other by 120° are usually used to feed the circulator.

Numerous studies are available in the literature for designing ferrite circulators [12]–[17]. For Y-junction stripline circulators, the work of Bosma [18], [19] forms the basis for theoretical studies. Much research work has built on these studies, including Fay and Comstock [20], [21] who proposed

Manuscript received 22 February 2022; revised 31 March 2022; accepted 18 April 2022. Date of publication 24 May 2022; date of current version 1 July 2022. This work was supported by the French Defence Innovation Agency. (*Corresponding author: Vincent Olivier.*)

Vincent Olivier, Bertrand Lenoir, Hamza Turki, and Christophe Breuil are with Inoveos, 19100 Brive-La-Gaillarde, France (e-mail: volivier@inoveos.com; b.lenoir@inoveos.com; hturki@inoveos.com; cbreuil@inoveos.com).

Thierry Monediere and Laure Huitema are with the Antennas and Signal Department, XLIM Research Institute, University of Limoges, 87000 Limoges, France (e-mail: thierry.monediere@unilim.fr; laure.huitema@unilim.fr).

Philippe Pouliguen is with the French Defence Innovation Agency, 75015 Paris, France.

Color versions of one or more figures in this article are available at <https://doi.org/10.1109/TMTT.2022.3175168>.

Digital Object Identifier 10.1109/TMTT.2022.3175168

0018-9480 © 2022 IEEE. Personal use is permitted, but republication/redistribution requires IEEE permission. See <https://www.ieee.org/publications/rights/index.html> for more information.

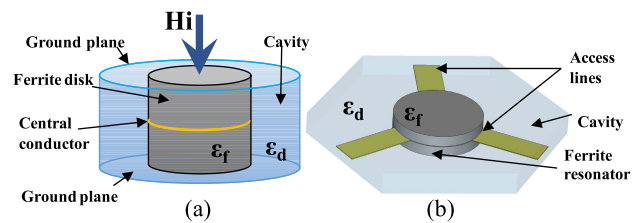


Fig. 1. (a) Ferrite resonator model and (b) basic stripline ferrite circulator model.

a method for designing ferrite circulators in the weak field. These works have shown how to extract the input impedance of a circulator as a function of its parameters [22], [23] (ferrite disk radius, the saturation magnetization, and the applied magnetic field). However, these methods are only valid when the central conductor considered is a disk of the same diameter as the ferrite disks. Moreover, authors often approximate the ferrite–dielectric boundary as a perfect magnetic wall.

More recent work [24] shows more accurate studies since the fields of the access stripline are considered. However, this study is only valid for a central conductor with a disk shape. Other methods of designing stripline circulators investigate different shapes of central conductors such as WYE or triangles [25]–[27]. These design methods are valid for the shape of the central conductor considered in each of the papers but cannot be generalized to other types of central conductors. This implies that many circulators with a complex central conductor geometry are designed by an iterative process using electromagnetic (EM) simulation software [10], [11], [25]. This nevertheless provides good performance but at the expense of simulation time.

However, the use of central conductors with different and optimized geometries can be relevant. Indeed, changing the shape of the central conductor offers the possibility to change the operating frequencies of a circulator and to offer circulators operating simultaneously on two frequency bands [11]. The studies presented in this article are a continuation of the article [11] and present a more general method for coupling a circulator. The term coupling used in this article means that we will focus on obtaining an optimal circulation phenomenon, i.e., combining both good impedance matching and good isolation on a given frequency or frequencies.

Our latest approaches already presented in [10] and [11] suggest to split the design of a ferrite circulator into two distinct steps.

First, the first step consists in performing an eigenmode analysis to determine the characteristics of the whole ferrite resonator (the saturation magnetization $4\pi Ms$ and the internal magnetic field Hi of the ferrites, their dimensions, the shape of the central conductor, and so on) that meets the initial specifications of the operating frequencies. For this purpose, this study is based on abacuses such as those presented in [11] and the objective is to have pairs of counter-rotating modes located around the desired operating frequencies. Thus, the first and second working frequencies of a dual-band circulator will appear between the resonance frequencies of the $HE_{\pm 11}$ and $HE_{\pm 21}$ [11].

At the end of this step, the geometrical parameters of the whole ferrite resonator, including the metallic part, i.e., the central conductor (the so-called central conductor is the totality of the metallic parts between the two ferrite disks) and the intrinsic characteristics of the ferrites are fixed.

Second, the second step is the coupling of the circulator, i.e., combining both good impedance matching and good isolation, by determining the dimensions of the access lines. An iterative parametric study is usually necessary and requires several simulations, which implies that the design time is greatly increased, especially for dual-band devices. In [10] and [11], the dimensions of the external access lines to the resonator are determined exclusively by a parametric study using EM simulation software. Furthermore, and especially for dual-band circulators, parametric studies may imply that the best solution is not found.

At the end of this step, the pairs of counter-rotating modes can be coupled and the circulation phenomenon appears approximately at the midfrequency of each pair. However, the coupling of these modes is done iteratively and is therefore not optimal.

On the basis of this observation, this article will present a new method for establishing optimal coupling conditions for a stripline circulator regardless of its geometry and this over several frequency bands simultaneously. This avoids any systematic numerical parametric studies and allows to reach the optimal coupling impedance of the junction.

This proposed new methodology is divided into two main parts:

- 1) the determination of the impedance matrix at the ferrite/dielectric interface;
- 2) the design of an optimal coupling/matching circuit.

Section II details the two parts of this new methodology. It will start with the calculation of the impedance matrix at the ferrite/dielectric interface using two different approaches. The first uses the integration of electric and magnetic fields to compute the impedance matrix at the interface. The second has the same objective and develops a deembedding method.

This impedance matrix at the ferrite/dielectric boundary will then be equalized to the impedance matrix of an ideal three-port circulator. Finally, the resulting equations will be used to determine both the width and length of the access lines to ideally couple the circulator and highlight the circulation

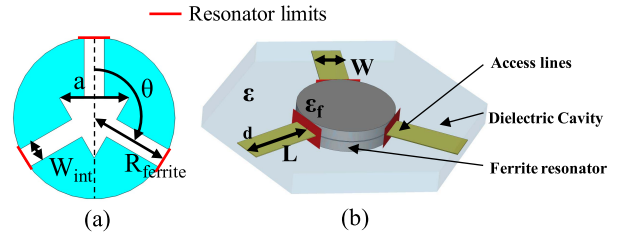


Fig. 2. (a) Shape of the central conductor (triangle surrounded by lines) in the ferrite disk resonator: ($\epsilon_r = 13$, $4\pi Ms = 2400$ G, $Hi = 700$ Oe, $R_{ferrite} = 3.2$ mm, $W_{int} = 0.8$ mm, $a = 2.8$ mm, $\theta = 2\pi/3$ rad, and thickness of ferrite disks is $t = 1.5$ mm). (b) Stripline circulator model and access lines dimensions W and L .

phenomenon. The last part of Section II will be devoted to the validation of the methodology presented above by measuring a prototype single-band circulator. The two approaches to the impedance matrix calculation will be discussed and compared, allowing us to choose the most appropriate option.

This methodology will be investigated in an even more complex case in Section III since we will apply it, for the first time, to a circulator operating on two different frequency bands without seeking to widen the bandwidth. Two examples of dual-band circulators will be presented and results from our methodology will be compared with the measurements.

II. COUPLING METHOD FOR STRIPLINE CIRCULATORS

A. Resonator Impedance Matrix Computation

In most cases, the extraction of an impedance matrix on a specific plane is very easy using the waveguide ports of EM simulation software when the materials used are isotropic. However, since ferrites are anisotropic materials, no EM simulation software supports waveguide ports on this type of material. Thus, this paragraph is dedicated to the calculation of the impedance matrix at the interface between the ferrite resonator and the surrounding dielectric using two different approaches. This matrix will be noted Z_R and is defined in the following equation:

$$[Z_R] = \begin{bmatrix} Z_{R11} & Z_{R12} & Z_{R13} \\ Z_{R21} & Z_{R22} & Z_{R23} \\ Z_{R31} & Z_{R32} & Z_{R33} \end{bmatrix}. \quad (1)$$

This section will take as an example the design shown in Fig. 2(a), arbitrarily chosen with a noncommon central conductor, i.e., never studied analytically in the literature. Even if the example of geometry used is a triangular central conductor, the methodology is suitable for all shapes.

The objective of this example will be to present the coupling (obtaining a circulation phenomenon, i.e., combining both good impedance matching and good isolation) of a resonator around 7.8 GHz. For this purpose, our method starts with the modal analysis of the structure. These modal analyses are similar to those presented in [11] and allow us to determine the internal static magnetic field of the ferrite, the properties and dimensions of the ferrite, as well as the dimensions of the central conductor in order to have a circulation phenomenon at the previously fixed frequency. These studies are not detailed here for reasons of compactness but lead to the dimensioning of the resonator, which consists of two ferrite disks (Fig. 2)

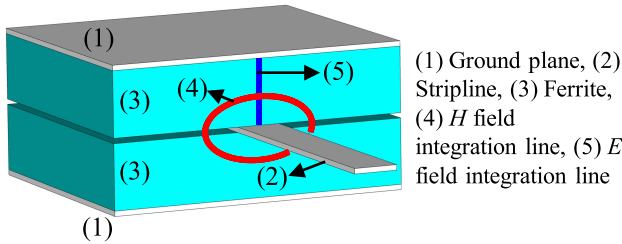


Fig. 3. E - and H -fields integration areas on stripline.

and a central conductor. What is called the central conductor in our study includes the whole metal part between the two ferrites, i.e., a triangle connected to three access lines. For a central conductor different from a disk with a diameter equal to ferrite disks, we consider the access lines in the ferrite as part of the resonator [Fig. 2(a)]. Indeed, works presented in [11] have shown that access line dimensions are relevant, especially for dual-band operation.

To obtain $HE_{\pm 11}$ fundamental modes around 7.8 GHz, an internal static magnetic field of 700 Oe has been determined as well as the properties and dimensions of the ferrites and central conductor, as shown in Fig. 2(a).

Fig. 2 also shows the planes (highlighted in red) in which the Z_R matrix will be calculated.

1) *E- and H-Fields Integration Method*: The first method to determine the Z_R impedance matrix consists in using the E - and H -fields at the interface between the ferrite resonator and the surrounding dielectric at the three circulator accesses (Fig. 2).

EM computations are done with CST Microwave Studio software (CST MWS), which does not allow the integration of excitation ports when these are connected to an anisotropic material. However, it is possible to compute and export both E - and H -fields values anywhere within the simulation bounding box, which will then be used to calculate the Z_R impedance matrix.

This method first consists in performing an EM simulation [Fig. 2(b)] of the resonator with access lines of arbitrary dimensions. By integrating the fields around striplines at the ferrite/dielectric interface, it is possible to obtain the voltage and current values at each interface. Indeed, if we consider a single stripline, it is possible to calculate voltage and current in a plane orthogonal to the direction of propagation due to the E - and H -fields [28]. Their expressions [28] when considering TEM modes propagating along a stripline are recalled in the following equations:

$$I = \oint \vec{H} \cdot d\vec{l} \quad (2)$$

$$V = \int \vec{E} \cdot d\vec{l}. \quad (3)$$

The current I is determined by integrating the H -field (2) around the stripline (red line in Fig. 3). The voltage is obtained by integrating the E -field between the upper (or lower) ground plane and the stripline (blue line in Fig. 3) [28].

This numerical method enables the calculation of I and V and is done at each access (ferrite/dielectric interface) of the circulator [highlighted in red in Fig. 4(a)]. It is, therefore,

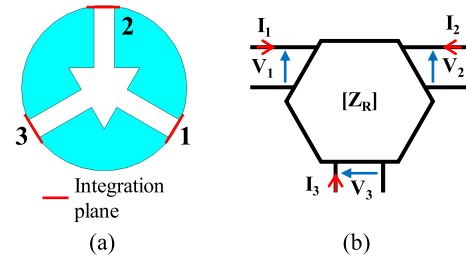


Fig. 4. Integration planes for computing (a) I and V of a ferrite resonator with a triangular central conductor and (b) I and V schematic representation for a three-port network.

possible to compute values of $V_{1,2,3}$ and $I_{1,2,3}$, i.e., the values of voltages and currents in planes 1, 2, and 3 [Fig. 4(b)].

Equation (4) is the relationship between values $V_{1,2,3}$ and $I_{1,2,3}$ and the terms of the impedance matrix Z_R of a three-port network [Fig. 4(b)]

$$\begin{pmatrix} V_1 \\ V_2 \\ V_3 \end{pmatrix} = \begin{bmatrix} Z_{R11} & Z_{R12} & Z_{R13} \\ Z_{R21} & Z_{R22} & Z_{R23} \\ Z_{R31} & Z_{R32} & Z_{R33} \end{bmatrix} \begin{pmatrix} I_1 \\ I_2 \\ I_3 \end{pmatrix}. \quad (4)$$

Considering that the three-port network is nonreciprocal and symmetrical, (5) is established

$$\begin{aligned} Z_{R11} &= Z_{R22} = Z_{R33} \\ Z_{R12} &= Z_{R23} = Z_{R31} \\ Z_{R21} &= Z_{R13} = Z_{R32}. \end{aligned} \quad (5)$$

From (4) and (5), the expressions of Z_{R11} , Z_{R21} , and Z_{R31} can be expressed as functions of $V_{1,2,3}$ and $I_{1,2,3}$. They are presented in the following equations:

$$Z_{R11} = \frac{1}{I_3} [V_3 - Z_{R31}I_1 - Z_{R21}I_1] \quad (6)$$

$$Z_{R21} = \frac{1}{I_1 - \frac{I_2^2}{I_3}} \left[V_2 - \frac{I_2}{I_3}V_3 - Z_{31} \left(I_3 - \frac{I_2^2}{I_3} \right) \right] \quad (7)$$

$$Z_{R31} = \frac{\left(V_1 - \frac{I_1}{I_3}V_3 \right) - \frac{\left(I_3 - \frac{I_1 I_2}{I_3} \right)}{\left(I_1 - \frac{I_2^2}{I_3} \right)} \left(V_2 - \frac{I_2}{I_3}V_3 \right)}{\left(I_2 - \frac{I_2^2}{I_3} \right) - \frac{\left(I_3 - \frac{I_1 I_2}{I_3} \right)}{\left(I_1 - \frac{I_2^2}{I_3} \right)} \left(I_3 - \frac{I_2^2}{I_3} \right)}. \quad (8)$$

The method of extracting $V_{1,2,3}$ and $I_{1,2,3}$ with the integration of the E - and H -fields at each access is applied on the complex resonator presented in Fig. 2(a). The results are plotted in Fig. 5.

The results presented in Fig. 5 required only one EM simulation. However, this is a plot over a wide frequency band, which therefore requires the extraction and calculation of the E - and H -fields of the complete structure at each of the frequency samples. The computation time is therefore long since, for Fig. 5, 1101 frequency samples were used. Indeed, the 3-D E - and H -fields have been computed at each of the 1101 frequency samples instead of about 20 for a standard 3-D EM simulation.

A second method of calculating the Z_R -matrix was also studied and is presented in the following.

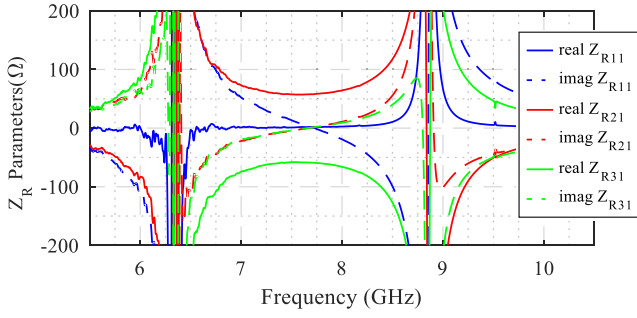


Fig. 5. Z_R -matrix calculated using the E and H integration method of the complex resonator presented in Fig. 2(a).

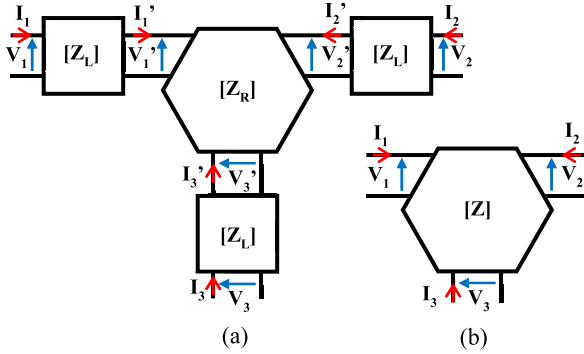


Fig. 6. Schematic representation of (a) complete system with the resonator and the three access lines and (b) its simplification into a single three-port network.

2) *Deembedding-Type Method*: In this section, a second extraction method of the three-port ferrite resonator Z -matrix is presented. This method consists, such as the previous one, in performing only one EM simulation of the resonator connected to three access lines with arbitrary characteristics.

Using this simulation and the characteristics of the access lines, the Z_R -matrix of the ferrite resonator is computed at its interface using a three-port deembedding method.

Indeed, a circulator is a three-port network composed of the ferrite resonator (which is itself a three-port network) connected to three two-port networks that are the access lines (Fig. 6).

The voltage–current relations of the whole system [Fig. 6(b)] are given by the following equations:

$$\begin{aligned} V_1 &= Z_{11} \times I_1 + Z_{31} \times I_2 + Z_{13} \times I_3 \\ V_2 &= Z_{21} \times I_1 + Z_{11} \times I_2 + Z_{31} \times I_3 \\ V_3 &= Z_{31} \times I_1 + Z_{21} \times I_2 + Z_{11} \times I_3 \end{aligned} \quad (9)$$

$$\text{Or } [V] = [Z][I]. \quad (10)$$

Likewise, the voltage–current relations of the ferrite resonator [Fig. 6(a)] at the ferrite/dielectric interface are given, as a function of Z_R , by the following equations:

$$\begin{aligned} V_1' &= Z_{R11} \times I_1' + Z_{R31} \times I_2' + Z_{R13} \times I_3' \\ V_2' &= Z_{R21} \times I_1' + Z_{R11} \times I_2' + Z_{R31} \times I_3' \\ V_3' &= Z_{R31} \times I_1' + Z_{R21} \times I_2' + Z_{R11} \times I_3' \end{aligned} \quad (11)$$

$$\text{Or } [V'] = [Z_R][I']. \quad (12)$$

Equation (13) gives the voltage–current relations for the three access two-port network with $n = 1, 2, \text{ and } 3$

$$\begin{aligned} V_n &= Z_{L11} \times I_n - Z_{L21} \times I_n' \\ V_n' &= -Z_{L11} \times I_n' + Z_{L21} \times I_n. \end{aligned} \quad (13)$$

Using (10), (12), and (13), we can write

$$[V'] = Z_{L21}[I] - \frac{Z_{L11}^2}{Z_{L21}}[I] + \frac{Z_{L11}}{Z_{L21}}[V] \quad (14)$$

$$[I'] = \frac{Z_{L11}}{Z_{L21}}[I] - \frac{1}{Z_{L21}}[V]. \quad (15)$$

Also, with (10), (14), and (15), it gives by the following equation:

$$\begin{aligned} \left(Z_{L21} - \frac{Z_{L11}^2}{Z_{L21}} \right) [I] + \frac{Z_{L11}}{Z_{L21}} [Z][I] \\ = [Z_R] \left(\frac{Z_{L11}}{Z_{L21}} [I] - \frac{1}{Z_{L21}} [Z][I] \right). \end{aligned} \quad (16)$$

Finally, from (16), the expression of Z_R is deduced

$$[A] = \left(Z_{L21} - \frac{Z_{L11}^2}{Z_{L21}} \right) [i] + \frac{Z_{L11}}{Z_{L21}} [Z] \quad (17)$$

$$[B] = \left(\frac{Z_{L11}}{Z_{L21}} [i] - \frac{1}{Z_{L21}} [Z] \right) \quad (18)$$

$$[Z_R] = [A][B]^{-1} \quad (19)$$

where $[i]$ is the identity matrix of order 3.

Therefore, the Z_R matrix (19) depends on the Z -matrix (the impedance matrix of the whole system) and on the access lines parameters Z_{L11} and Z_{L21} . The latter can be expressed as a function of Z_c , the stripline characteristic impedance, its length L , and the frequency [28]. They are recalled in the following equations:

$$Z_{L11} = -jZ_c \times \cot(L\omega) \quad (20)$$

$$Z_{L21} = \frac{-jZ_c}{\sin(L\omega)}. \quad (21)$$

Z_c and L are fixed by the access lines used in the simulation and the Z -matrix is extracted from this same EM simulation of the entire system.

Finally, we can deduce the Z_R impedance matrix of the ferrite resonator at the interface ferrite/dielectric due to this unique EM simulation.

This deembedding-type method is applied on the structure described in Fig. 2(a) and the Z_R -matrix elements are presented in Fig. 7. This 3-D EM simulation was performed under CST MWS, with access line properties of $Z_c = 50 \Omega$ and $L = 5 \text{ mm}$. It should be noted that these line characteristics were chosen arbitrarily and could be different. In each case, the Z_R -matrix results would be identical.

3) *Comparison of the Two Methods*: Fig. 8 shows a comparison of the Z_R -matrix of the resonator shown in Fig. 2(a) calculated with the E/H integration method and with the deembedding-type method. The two results are very close, and they both show a resonance around the frequencies of 6.3 and 8.9 GHz. These frequencies correspond to the resonant frequencies of the counter-rotating eigenmodes in the cavity.

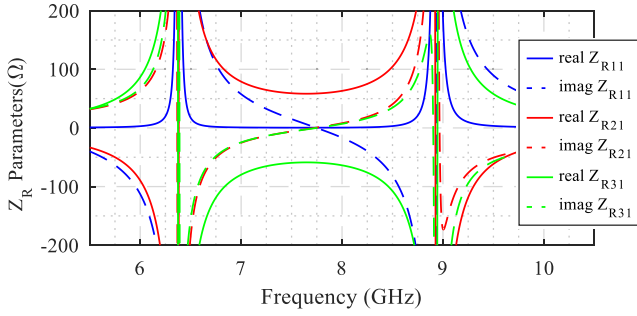


Fig. 7. Z_R -matrix calculated using the deembedding-type method of the complex resonator presented in Fig. 2(a).

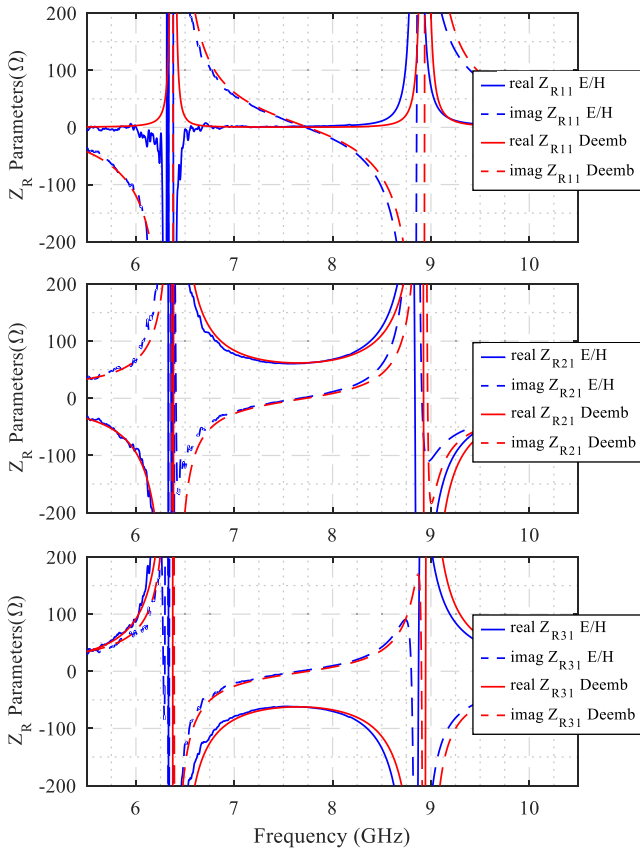


Fig. 8. Comparison of the Z_R -matrix of the complex resonator presented in Fig. 2(a) calculated using the E/H integration method and deembedding-type method.

At this stage, we have determined the Z_R impedance matrix at the ferrite/dielectric interface, regardless of the shapes of the metallic central conductor and the ferrite resonator. In Section II-B, this Z_R matrix will be made equal to the impedance matrix of an ideal three-port circulator. This will allow us to determine the width and length of the access lines to ideally couple the circulator and highlight the circulation phenomenon.

B. Use of the Z_R Impedance Matrix to Ideally Couple the Circulator

The Z_R -matrix computation at the ferrite/dielectric interface was the first step of the coupling methodology.

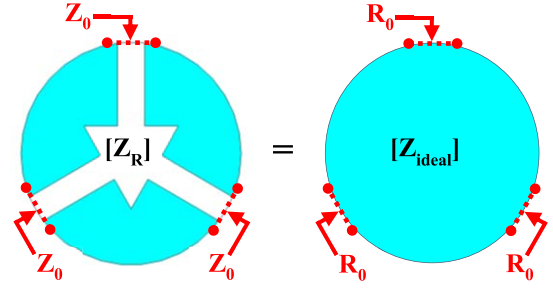


Fig. 9. Schematic representation of obtaining an ideal circulation condition for the circulator under study.

The purpose of the second step, presented in this section, is to determine the characteristics of the access lines that will allow an optimized coupling of the eigenmodes of the ferrite resonator, i.e., that will lead to a good matching ($S_{11} < -20$ dB), low losses ($S_{21} < -1$ dB), and a good isolation ($S_{31} < -20$ dB).

For this purpose, the starting point is to equalize the impedances of the previously studied circulator with those of an ideal circulator.

The impedance matrix of an ideal circulator, noted Z_{ideal} in the following, has already been defined in previous works [18] and is recalled in the following equation:

$$[Z_{ideal}] = \begin{bmatrix} 0 & -R_0 & R_0 \\ R_0 & 0 & -R_0 \\ -R_0 & R_0 & 0 \end{bmatrix}. \quad (22)$$

This implies that the impedances at each of the input ports of the ideal circulator are real and equal to R_0 . We note Z_0 the impedances at each of the input ports of the previously studied circulator. Consequently, and in order to obtain an optimized circulation phenomenon in the case of the circulator studied previously, Z_0 must be a real impedance at the circulation frequency, which we will note f_0 in the following. This ideal circulation condition is schematized, in a simplified way, by an equal sign in Fig. 9.

This impedance Z_0 is defined as the ratio (23) between the voltage and current on port 1 when the other ports are loaded by the same impedance Z_0 . It is calculated with the Z_R -matrix (previously determined according to Section II-A) of the resonator using (24)–(26)

$$Z_0 = \frac{V_1}{I_1} \quad (23)$$

$$Z_0 = Z_{R11} + E Z_{R31} + Z_{R21} F \quad (24)$$

$$E = \frac{Z_{R21} + \frac{Z_{R31}^2}{-Z_0 - Z_{R11}}}{-Z_0 - Z_{R11} - \frac{Z_{R21} Z_{R31}}{-Z_0 - Z_{R11}}} \quad (25)$$

$$F = \frac{Z_{R31}}{-Z_0 - Z_{R11}} + E \left(\frac{Z_{R21}}{-Z_0 - Z_{R11}} \right). \quad (26)$$

From these equations and keeping only the solutions with a positive real part, Fig. 10 presents the real and imaginary parts of the solution Z_0 as a function of frequency.

These curves show that there is one frequency around which the impedance Z_0 is purely real, i.e., which meets the ideal circulation condition (shown in Fig. 9). This frequency, where

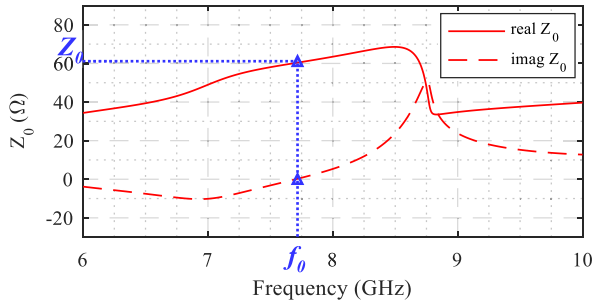


Fig. 10. Real and imaginary parts of the Z_0 solution (23)–(26) as a function of frequency for the resonator presented in Fig. 2(a).

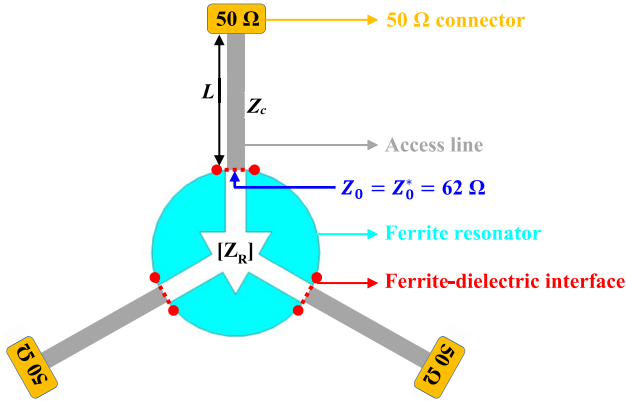


Fig. 11. Resonator and access lines loaded by 50-Ω ports.

$Z_0 = 62 \Omega$, is the circulation frequency, and it is such that $f_0 = 7.7$ GHz.

In a practical case, the circulator is connected to 50-Ω connectors. In general, impedance matching is performed when the load impedance equals the complex conjugate of the source impedance. Therefore, to perfectly match the circulator at the circulation frequency f_0 , the conjugate of Z_0 , noted Z_0^* , has to be presented by the access line loaded by the 50-Ω connector, as shown in Fig. 11. Here, at f_0 , Z_0 is purely real, which implies that $Z_0^* = Z_0 = 62 \Omega$.

Therefore, in the overall system presented in Fig. 11, the characteristics of the access lines, i.e., its characteristic impedance Z_c and its length L , have to be determined to have an impedance of 62Ω at each ferrite–dielectric interface at the frequency f_0 .

These lines are striplines with continuous section and the dielectric around the ferrite is air. In order to obtain a real impedance of 62Ω in the plane of the ferrite–dielectric interface, these lines can be quarter-wave impedance transformers. In this case, the length L and the characteristic impedance Z_c of the access lines are defined as follows:

$$L = \frac{c}{4f_0} \quad \text{and} \quad Z_c = \sqrt{50 \times 62} = 56 \Omega \quad (27)$$

where c is the velocity of light.

The width of the access lines that allows a characteristic impedance of 56Ω is 3.5 mm.

Now that all system elements are defined, it is possible to determine the S -matrix of the complete circulator. Using (10), (12), and (13) again, it is possible to develop them in order to find an expression of the impedance matrix Z of the

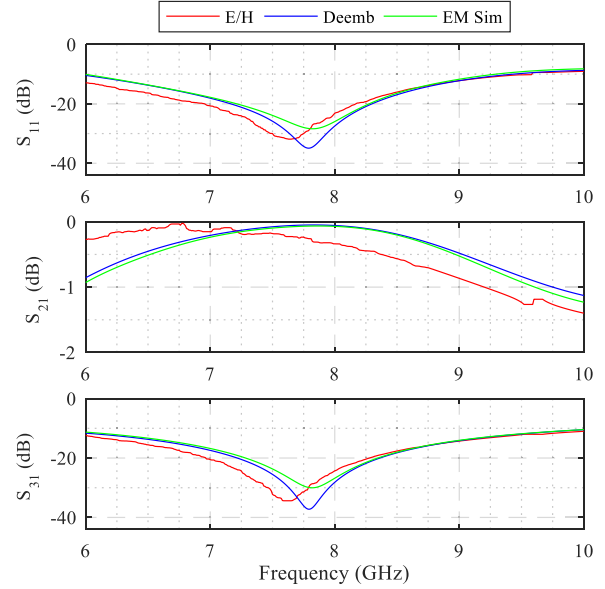


Fig. 12. S -matrix of the resonator with $\lambda/4$ lines sections computed with the E and H integration method (E/H), with deembedding method (Deemb), and with 3-D EM simulation using Fig. 2(b) model (EM Sim).

entire system. This expression depends on the Z_R -matrix of the resonator and the properties of the access lines, Z_c and L . Equations (28)–(30), which allow the calculation of the impedance matrix Z of the overall system, are thus defined

$$[C] = \left(\frac{Z_{L11}}{Z_{L21}}[i] + [Z_R] \frac{1}{Z_{L21}} \right) \quad (28)$$

$$[D] = \frac{Z_{L11}}{Z_{L21}}[Z_R] - \left(Z_{L21} - \frac{Z_{L11}^2}{Z_{L21}} \right)[i] \quad (29)$$

$$[Z] = [C]^{-1}[D]. \quad (30)$$

Z_{L11} and Z_{L21} can be calculated with (20) and (21). They depend on the frequency, the characteristic impedance Z_c , and the length L of the stripline.

Finally, (31) is used to convert the Z -matrix into an S -matrix [28]

$$[S] = \left(\frac{1}{Z_0}[Z] + [i] \right)^{-1} \left(\frac{1}{Z_0}[Z] - [i] \right). \quad (31)$$

Thus, using (28)–(31), the S -matrix of the complete circulator can be calculated. Since we have determined the Z_R -matrix of the ferrite resonator with two different methods (Section II-A), Fig. 12 shows the S -matrix when the following conditions hold.

- 1) The Z_R matrix of the ferrite resonator is calculated using the “ E and H ” integration method.
- 2) The Z_R matrix of the ferrite resonator is calculated using the deembedding method.
- 3) The 3-D EM simulation of the entire circulator is performed.

The results show that, as predicted by the previously developed methodology, a circulation phenomenon around 7.7 GHz is obtained with very good isolation and matching while having very low losses. Moreover, results obtained using the two methods are very close with a frequency difference of 2.6%.

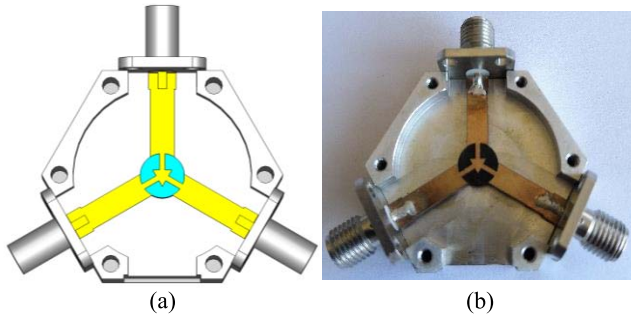


Fig. 13. Lower part of the circulator with a triangular central conductor: (a) numerical model and (b) prototype.

These results are also compared to an EM simulation using a 3-D model of the circulator with the dimensions of the access lines previously determined. This comparison shows a very good agreement between the two computation methods and the simulation.

The strong point of this method is that to design this circulator, only one simulation is necessary and no parametric study is required. This design methodology must now be validated experimentally.

C. Experimental Validation and Methods Comparison

In order to validate the design methodology, a prototype is developed. The topology used is the one determined at the end of Section II-B. The ferrite initially considered had an internal field of 700 Oe [Fig. 2(a)]. Therefore, to complete the design of the circulator, a magnetostatic study is carried out in order to select the magnets that allow to obtain the internal static magnetic field of 700 Oe in the ferrite disks. Indeed, due to the CST magnetostatic solver (MS), magnets can be dimensioned to achieve an internal field as close as possible to the wanted one. These magnetostatic studies have already been presented in [10] and [11]. The magnets thus dimensioned are 3-mm high disks with a radius of 4.5 mm and a B_r magnetization of 4000 G.

A magnetostatic–EM (MS/EM) cosimulation of the global device [Fig. 13(a)] is done (using CST MWS) in order to verify the results given by both methods presented in Section II.

Finally, the circulator is realized and the photograph of its prototype is shown in Fig. 13(b). It has been measured and Fig. 14 shows a comparison between the MS/EM cosimulation and measurements. We can see a good agreement between the measurement and the MS/EM cosimulation.

The most important part of this section is to validate the methodologies presented previously. For this purpose, Fig. 15 compares the measurements results with those calculated using the two methods of determining the Z_R -matrix (in Sections II-A and II-B). Indeed, Fig. 15(a) shows the results from the E and H integration method and Fig. 15(b) shows the results from the deembedding method. In both cases, a good agreement appears particularly between the deembedding method and the measurements. Table I summarizes the results, including the results from the 3-D simulation in the ideal case where the internal field was homogeneous.

The two methods developed are, therefore, validated since a very good agreement with the measurements is obtained.

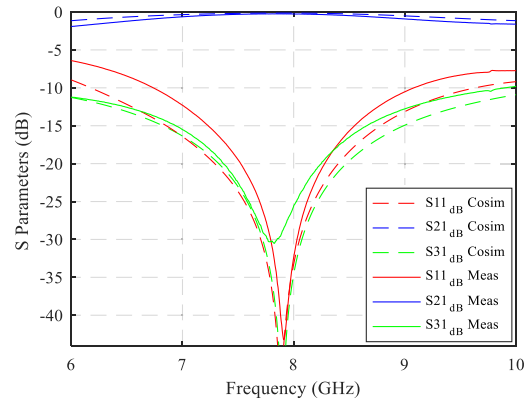


Fig. 14. Comparison of the S -parameters from the MS/EM cosimulation of the 3-D model shown in Fig. 13(a) and from measurements of the prototype presented in Fig. 13(b).

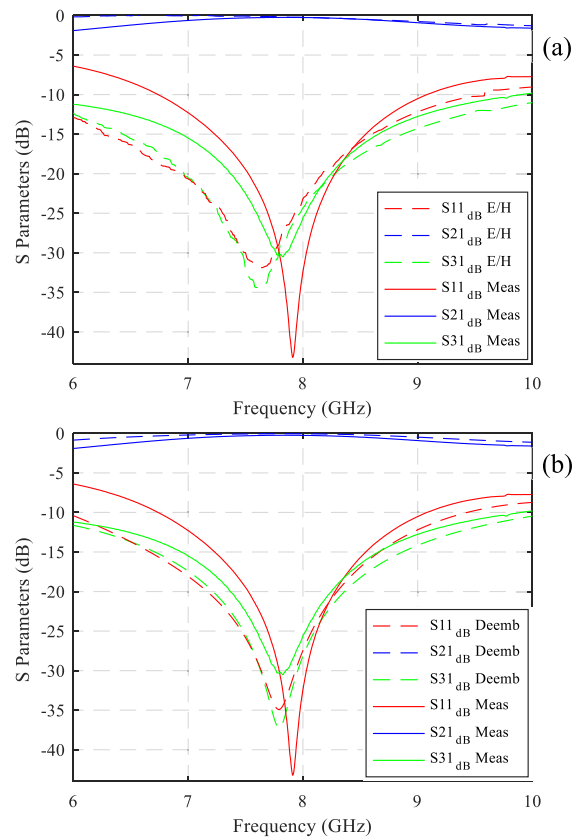


Fig. 15. Comparison of the S -matrix of the circulator (a) between the measurements and the E/H integration method and (b) between the measurements and the deembedding method.

It should be noted that the agreement is better for the deembedding method.

The most significant advantage of this global methodology, the results of which are presented in Fig. 15, is that it requires only a single EM simulation of an unmatched circulator. The rest of the methodology is just combinations of matrices whose objective is to obtain a circulation close to an ideal circulator. In this overall methodology, we used two different methods to calculate the elements of the Z_R -matrix.

In the first method (called E and H integration method), the calculation time is much more important than in the second

TABLE I
PERFORMANCE COMPARISON

Results	E/H Method	Deemb Method	EM Sim	MS/EM Cosim	Measures
Central frequency (GHz)	7.56	7.76	7.78	7.86	7.88
BW (%) Iso > 20dB and RL > 20dB	15.9	13.9	12.8	13.7	9.1
Relative deviation (%)	4.1	1.5	1.3	0.3	/
Computation time (s)	6733	69	157	312	/

one (deembedding method) because it is necessary to calculate the E - and H -fields in 3-D for each frequency sample.

Indeed, to obtain the results of Section II-B with a standard computer (Intel i7 quadricore CPU at 3.4 GHz, RAM 16 Go and GPU NVIDIA GeForce GTX 745), the total computation time was 6733 s for the E and H integration method and 69 s for the deembedding method. Thus, with an error of 1.5% versus 4.1% on the central circulation frequency and computing times divided by 100, the deembedding method will be preferred thereafter.

Now that the methodology developed in this article has been validated in the case of a single-band circulator, the next part will show that it can be implemented in more complex cases since we will apply it to a circulator operating on two different frequency bands without seeking to widen the bandwidth.

Indeed, it should be noted that the bandwidth of the circulators depends essentially on the evolution of Z_0 with frequency. With a resonator whose real part of Z_0 varies slightly with frequency and an imaginary part of Z_0 close to 0, it would be possible to obtain larger bandwidths.

III. APPLICATION OF THE METHODOLOGY FOR A DUAL-BAND CIRCULATOR

In this section, the coupling methodology is adapted and applied to obtain an optimized dual-band circulator. Indeed, for dual-band circulators presented in [10] and [11], design methods required an iterative parametric study to design the access lines of the ferrite resonator.

In [8], the influence of the shape of the central conductor on the resonant frequencies of the eigenmodes has been detailed and it was shown that it is necessary to use conductors of complex shapes to obtain resonant modes at the desired operating frequencies. However, the dimensions of the access lines, to couple and match the resonator to obtain an optimized circulation function on both frequency bands, were calculated by an iterative parametric study (using CST-MWS) [11]. The aim of this optimization was to find an optimal coupling in the two circulation bandwidths. This technic is long and tedious and requires significant computing time for each new design. This is the reason why we propose, in this section, to apply the method previously proposed for a dual-band conception.

This new method has been applied on the two circulators already realized and presented in [11]. Each of them has cylindrical ferrite resonators with central conductors WYE

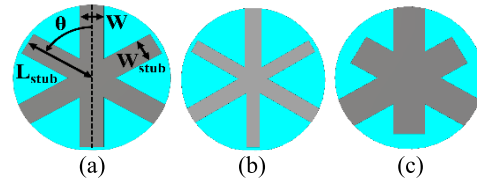


Fig. 16. (a) WYE with stubs central conductor shape, (b) for the unidirectional circulator, and (c) for the bidirectional circulator.

TABLE II
CIRCULATOR WITH WYE WITH STUBS CENTRAL CONDUCTOR PROPERTIES

Properties	Fig. 16(b) resonator	Fig. 16(c) resonator
W (mm)	1.5	2.8
Wstub (mm)	1.2	2.8
Lstub (mm)	6.2	5.2
Ferrite radius (mm)	6.6	
Ferrite thickness (mm)	1.5	

ended by stubs. The main difference between these two resonators concerns the dimensions of the lines and stubs of the WYE central conductor and was intended to change the order of appearance of the upper modes $HE_{\pm 21}$. This resulted in the inversion of the direction of the circulation since it could be either the same between the first and second bands (unidirectional circulator) or different (bidirectional circulator).

Fig. 16(b) and (c) shows the geometries of the central conductors corresponding to the two cases presented above.

The ferrite used is Y215 [29] with a saturation magnetization M_s of 1450 G and the internal static magnetic field H_i of the ferrite is 640 Oe for both resonators.

Table II shows the different dimensions of the ferrite resonators shown in Fig. 16.

The following paragraphs present the application of the coupling method described in Section II in order to optimally couple the resonators shown in Fig. 16(b) and (c) on two frequency bands.

A. Unidirectional Circulator

As for the single-band circulator, the first step consists in calculating the impedance matrix Z_R at the interface between the ferrite and the surrounding dielectric (which is air in our case).

The deembedding method is applied because of its greater precision and rapidity. First, a 3-D EM simulation is performed by exciting the resonator with access lines whose width is chosen arbitrarily. Then, the Z_R matrix is computed using (17)–(21). Fig. 17 shows the Z_R matrix of the resonator shown in Fig. 16(b).

These different curves show resonance peaks, which can be identified with the different modes present in the cavity and already presented in [11]. From the different elements of this impedance matrix Z_R , it is possible to calculate the Z_0 impedance defined in Fig. 9 with (24)–(26). From these

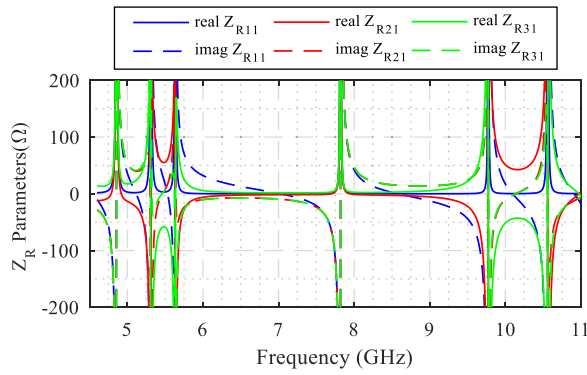


Fig. 17. Z_R -matrix calculated using the deembedding type method of the resonator presented in Fig. 16 (b).

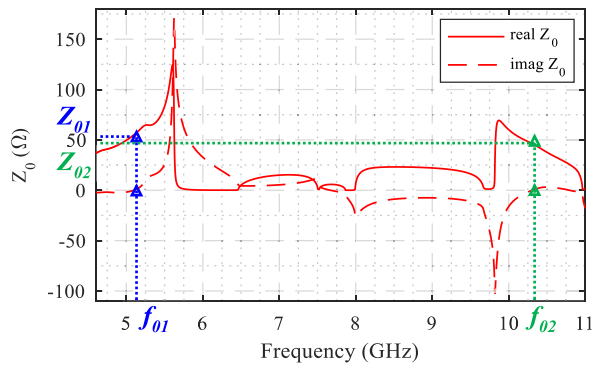


Fig. 18. Real and imaginary parts of the Z_0 solution (23)–(26) as a function of frequency for resonator presented in Fig. 16 (b).

equations and keeping only the solutions with a positive real part, Fig. 18 presents the real and imaginary parts of the solution Z_0 as a function of frequency. As for the single-band circulator, these curves show that it is possible to find frequencies where the impedance Z_0 is purely real, i.e., which meets the ideal circulation condition (shown in Fig. 19).

The main difference with dual-band operation is the search for two frequencies instead of one. Using the results of Z_0 (Fig. 18), the frequencies f_{01} and f_{02} at which Z_0 is purely real are identified and are such that $f_{01} = 5.1$ GHz and $f_{02} = 10.3$ GHz with the corresponding impedances $Z_{01} = 55 \Omega$ and $Z_{02} = 46 \Omega$.

Therefore, these values of Z_0 are both close to 50Ω , so we will consider that applying an impedance of 50Ω to the three ports will allow coupling the resonator at the frequencies of 5.1 and 10.3 GHz. Since the impedance to be applied is 50Ω , there is no need to add a matching section. The resonator can therefore be connected to connectors using characteristic impedance lines of 50Ω .

In order to compare the measurement results of [11] with those obtained with the methodology developed in this article, (28)–(31) are applied for the resonator of Fig. 16(b). Using the matrix Z_R shown in Fig. 17 and the properties of the access lines, i.e., $Z_c = 50 \Omega$ and $L = 5$ mm, the S -matrix of the coupled resonator is calculated as a function of frequency without requiring a new 3-D EM simulation. These results are compared with the measurements [11] in Fig. 19.

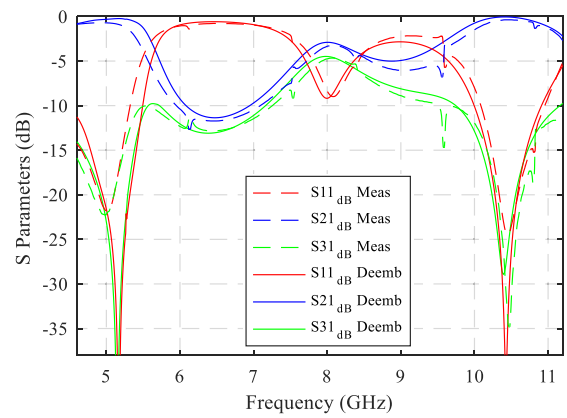


Fig. 19. Comparison of the S -matrix of the circulator between the measurements and the deembedding method.

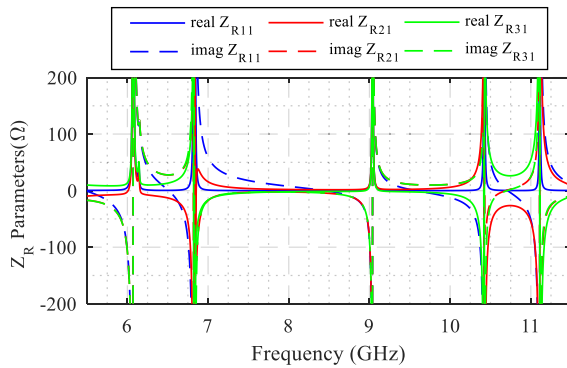


Fig. 20. Z_R -matrix calculated using the deembedding-type method of the resonator presented in Fig. 16(c).

Fig. 19 shows a good agreement between the measured and the calculated S -matrix. Retro simulations have shown that spurious peaks in measurements come from a minor misalignment of the ferrite disks.

B. Bidirectional Circulator

The same development is adapted for the resonator shown in Fig. 16(c). Indeed, the Z_R -matrix is calculated using the same method as for the previous part, with the deembedding method. The terms of this matrix are plotted in Fig. 20.

From this Z_R -matrix, the Z_0 impedance is computed using (23)–(26) and Fig. 21 shows its plot as a function of frequency.

As with the previous resonator (Section III-A), a dual-band circulation is targeted. For having a circulation phenomenon, it is necessary to identify the frequencies where the impedance Z_0 is purely real. These two frequencies for which the imaginary part of Z_0 is equal to zero are $f_{01} = 6.1$ GHz and $f_{02} = 10.6$ GHz. The corresponding impedances are $Z_{01} = 30 \Omega$ and $Z_{02} = 33 \Omega$.

It will therefore be considered that the resonator can be coupled by applying an impedance of 32Ω at 6.1 and 10.6 GHz to the three ports.

As this impedance is different from 50Ω , a matching step must be added to connect the resonator to the $50\text{-}\Omega$ connectors. Since the circulator must operate on the two frequency bands

TABLE III
COMPARISON BETWEEN CIRCULATOR DESIGN METHODS

	Proposed method	Fay & Comstock method [20]	Helszajn method [26]	Wu and Rosebaum method [1]	Shams <i>et al</i> method [24]
Resonator design included	No, need to use [11] modal study	Yes	Yes	Yes	Yes
Accuracy	Good accuracy, relative deviation of 1.5% (Table I)	Boundary approximation	Boundary approximation	Boundary approximation	Boundary approximation, stripline fields considered
Validity	For every central conductor shape	For a central conductor disk with weak bias field conditions	For a WYE resonator	For a central conductor disk and ferrite surrounded by dielectric	For a central conductor disk
Performance obtained	Narrow bandwidths, high isolation	Narrow bandwidths	Wide band	Ultra-wide band	Narrow bandwidths
Dual band allowed	Yes	No	No	No	No

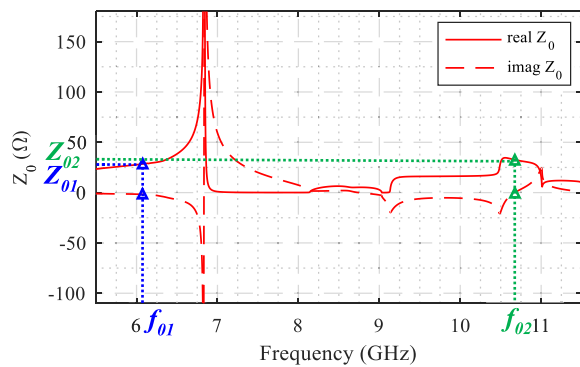


Fig. 21. Real and imaginary parts of the Z_0 solution (23)–(26) as a function of frequency for resonator presented in Fig. 16 (c).

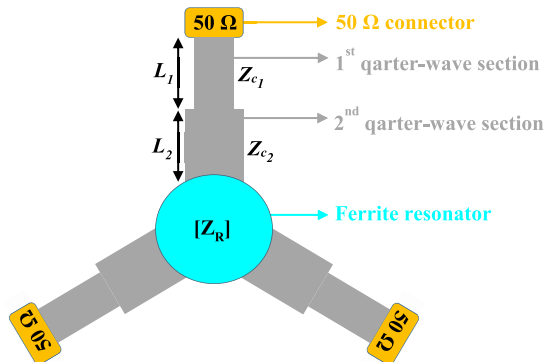


Fig. 22. Schematic representation of resonator connected to two matching sections and ports.

simultaneously, it is not possible to use a single quarter-wave impedance transformer to convert an impedance of 32 into 50 Ω at 6.1 and 10.6 GHz. A two quarter-wave section [30] can be used to match the resonator. The global system is represented in Fig. 22 with the resonator in the middle,

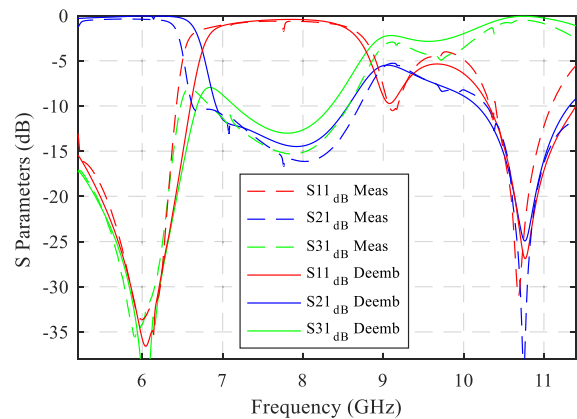


Fig. 23. Comparison of the S -matrix of the circulator between the measurements and the deembedding method.

connected to the two quarter-wave sections, and terminated by the 50- Ω connectors. This method, already detailed in [11], resulted in the following parameters: $Z_{c1} = 44 \Omega$, $Z_{c2} = 36 \Omega$, $L_1 = 9.15$ mm, and $L_2 = 9.15$ mm respecting the notations of Fig. 22.

It is, therefore, possible, by using (20), (21), and (28)–(31) and the matrix Z_R shown in Fig. 20, to calculate the S -matrix of the whole system. The results are compared with the measurements [11] in Fig. 23.

As with the previous circulators, in addition to good agreement between measurements and calculations, very good circulation performances are achieved. Indeed, the methodology developed in this article allows, from a single 3-D simulation, to develop circulators with a good matching, low losses, and good isolation on one or more frequency bands.

Table III summarizes the performance of the main ferrite circulator design methods. The method we propose in this article is compared to the method of Fay and Comstock [20], which is based on Bosma approximations [18], to the

method of Helszajn [26] using a WYE resonator to extend the bandwidths, to the ultrawideband method of Wu and Rosenbaum's [1] and to the method of Shams *et al.* [24], which considers the fields surrounding the access striplines to model a circulator.

We can deduce from this table that the method proposed in this article is the only one valid for any type of central conductor. To the best of the authors' knowledge, it is also the only one that allows to achieve a second circulation band without parametric studies.

IV. CONCLUSION

In this article, a new methodology has been introduced to obtain optimal circulation conditions for a stripline circulator, whatever its geometry, over several frequency bands simultaneously. It has been developed to avoid any systematic numerical parametric studies while reaching the optimal coupling impedance of the junction. For this purpose, a first step consisted in calculating the impedance matrix of the resonator, having an arbitrarily chosen central conductor, at the ferrite/dielectric interface. Two approaches have been developed. The first one used the integration of electric and magnetic fields, while the second developed a deembedding type method.

This impedance matrix of the resonator was then equalized to that of an ideal circulator to extract the impedance to be presented at each of its input ports to obtain the best circulation phenomenon. From this impedance, we can deduce the characteristics of the access lines, i.e., their characteristic impedance and their length. The methodology has been validated by measuring a single-band circulator with a triangular central conductor.

We have also proved that this methodology is also suitable for coupling a circulator on two frequency bands simultaneously. For this purpose, we used the results of two dual-band circulators already realized. Indeed, by applying our methodology, we have shown that by using a single EM simulation, coupling parameters on two different frequency bands were found instead of using a parametric study.

The most significant advantage of the methodology developed in this article is that, from a single 3-D simulation, we can develop circulators with good matching, low losses, and good isolation on one or more frequency bands. This new approach shows, in all the studied cases, that a good agreement between measurements and calculations is achieved. Finally, this method, presented here for stripline technologies, can be applied to microstrip technology.

ACKNOWLEDGMENT

This work has been done in the framework of the collaborative laboratory "INOGYRO," established between XLIM Research Institute, Limoges, France, and INOVEOS, Brive-La-Gaillarde, France.

REFERENCES

- [1] Y. S. Wu and F. J. Rosenbaum, "Wideband operation of microstrip circulators," in *Proc. IEEE G-MTT Int. Microw. Symp.*, Boulder, CO, USA, Jun. 1973, pp. 92–94, doi: [10.1109/GMTT.1973.1123103](https://doi.org/10.1109/GMTT.1973.1123103).
- [2] H. Turki, L. Huitema, T. Monediere, B. Lenoir, and C. Breuil, "Complete methodology of low-loss ultra-wideband junction circulator," in *IEEE MTT-S Int. Microw. Symp. Dig.*, Philadelphia, PA, USA, Jun. 2018, pp. 746–749, doi: [10.1109/MWSYM.2018.8439670](https://doi.org/10.1109/MWSYM.2018.8439670).
- [3] E. Benevent, T. Rouiller, B. Sauviac, V. Larrey, D. Vincent, and A. Madelaine, "Stripline Y-junction circulator using barium hexagonal ferrite thin films," in *Proc. IEEE Int. Symp. Ind. Electron.*, Ajaccio, France, vol. 1, May 2004, pp. 15–18, doi: [10.1109/ISIE.2004.1571773](https://doi.org/10.1109/ISIE.2004.1571773).
- [4] J. Wang *et al.*, "Self biased Y-junction circulator at K_u band," *IEEE Microw. Wireless Compon. Lett.*, vol. 21, no. 6, pp. 292–294, Jun. 2011, doi: [10.1109/LMWC.2011.2142297](https://doi.org/10.1109/LMWC.2011.2142297).
- [5] V. Laur *et al.*, "Self-biased Y-junction circulators using lanthanum- and cobalt-substituted strontium hexaferrites," *IEEE Trans. Microw. Theory Techn.*, vol. 63, no. 12, pp. 4376–4381, Dec. 2015, doi: [10.1109/TMTT.2015.2495218](https://doi.org/10.1109/TMTT.2015.2495218).
- [6] S. Yang, D. Vincent, J. R. Bray, and L. Roy, "Study of a ferrite LTCC multifunctional circulator with integrated winding," *IEEE Trans. Compon., Packag., Manuf. Technol.*, vol. 5, no. 7, pp. 879–886, Jul. 2015, doi: [10.1109/TCPMT.2015.2440660](https://doi.org/10.1109/TCPMT.2015.2440660).
- [7] A. Ashley, L. F. Marzall, Z. Popovic, and D. Psychogiou, "Frequency selective ferrite circulators with quasi-elliptic transmission response," in *Proc. 48th Eur. Microw. Conf. (EuMC)*, Madrid, Spain, Sep. 2018, pp. 211–214, doi: [10.23919/EUMC.2018.8541616](https://doi.org/10.23919/EUMC.2018.8541616).
- [8] V. Laur, J. P. Gouavogui, and B. Balde, "C-band hybrid 3-D-printed microwave isolator," *IEEE Trans. Microw. Theory Techn.*, vol. 69, no. 3, pp. 1579–1585, Mar. 2021, doi: [10.1109/TMTT.2021.3053277](https://doi.org/10.1109/TMTT.2021.3053277).
- [9] H. Razavipour, G. Askari, F. Fesharaki, and H. Mir mohammad-Sadeghi, "A new high-power, dual-band, E-plane, ferrite circulator," in *Proc. IEEE EUROCON*, St. Petersburg, Russia, May 2009, pp. 20–25, doi: [10.1109/EURCON.2009.5167598](https://doi.org/10.1109/EURCON.2009.5167598).
- [10] H. Turki, L. Huitema, T. Monediere, B. Lenoir, and C. Breuil, "New concept validation of low-loss dual-band stripline circulator," *IEEE Trans. Microw. Theory Techn.*, vol. 67, no. 3, pp. 845–850, Mar. 2019, doi: [10.1109/TMTT.2018.2890632](https://doi.org/10.1109/TMTT.2018.2890632).
- [11] V. Olivier *et al.*, "Dual-band ferrite circulators operating on weak field conditions: Design methodology and Bandwidths' improvement," *IEEE Trans. Microw. Theory Techn.*, vol. 68, no. 7, pp. 2521–2530, Jul. 2020, doi: [10.1109/TMTT.2020.2988003](https://doi.org/10.1109/TMTT.2020.2988003).
- [12] J. B. Davies and P. Cohen, "Theoretical design of symmetrical junction stripline circulators," *IEEE Trans. Microw. Theory Techn.*, vol. MTT-11, no. 6, pp. 506–512, Nov. 1963, doi: [10.1109/TMTT.1963.1125717](https://doi.org/10.1109/TMTT.1963.1125717).
- [13] J. W. Simon, "Broadband strip-transmission line Y-junction circulators," *IEEE Trans. Microw. Theory Techn.*, vol. MTT-13, no. 3, pp. 335–345, May 1965, doi: [10.1109/TMTT.1965.1125998](https://doi.org/10.1109/TMTT.1965.1125998).
- [14] J. Helszajn, *The Stripline Circulator: Theory and Practice*. Hoboken, NJ, USA: Wiley, 2008, p. 614.
- [15] M. T. Hickson, L. E. Davis, D. K. Paul, and D. Sillers, "Computer-aided design and optimisation of broadband stripline circulators for 1830 GHz and 1840 GHz," in *IEEE MTT-S Int. Microw. Symp. Dig.*, Boston, MA, USA, Jul. 1991, pp. 961–964, doi: [10.1109/MWSYM.1991.147169](https://doi.org/10.1109/MWSYM.1991.147169).
- [16] J. Helszajn, "Synthesis of octave-band quarter-wave coupled semi-tracking stripline junction circulators," *IEEE Trans. Microw. Theory Techn.*, vol. 43, no. 3, pp. 573–581, Mar. 1995, doi: [10.1109/22.372103](https://doi.org/10.1109/22.372103).
- [17] M. Pinto, L. Marzall, A. Ashley, D. Psychogiou, and Z. Popovic, "Design-oriented modelling of microstrip ferrite circulators," in *Proc. 48th Eur. Microw. Conf. (EuMC)*, Sep. 2018, pp. 215–218, doi: [10.23919/EUMC.2018.8541559](https://doi.org/10.23919/EUMC.2018.8541559).
- [18] H. Bosma, "On the principle of stripline circulation," in *Proc. IEE-B, Electron. Commun. Eng.*, vol. 109, no. 21S, pp. 137–146, Jan. 1962.
- [19] H. Bosma, "On stripline Y-circulation at UHF," *IEEE Trans. Microw. Theory Techn.*, vol. MTT-12, no. 1, pp. 61–72, Jan. 1964, doi: [10.1109/TMTT.1964.1125753](https://doi.org/10.1109/TMTT.1964.1125753).
- [20] C. E. Fay and R. L. Comstock, "Operation of the ferrite junction circulator," *IEEE Trans. Microw. Theory Techn.*, vol. MTT-13, no. 1, pp. 15–27, Jan. 1965, doi: [10.1109/TMTT.1965.1125923](https://doi.org/10.1109/TMTT.1965.1125923).
- [21] C. E. Fay and R. L. Comstock, "On the theory of the ferrite junction circulator," in *Proc. PTGMTT Int. Symp. Dig.*, Long Island, NY, USA, vol. 64, 1964, pp. 54–59, doi: [10.1109/PTGMTT.1964.1122423](https://doi.org/10.1109/PTGMTT.1964.1122423).
- [22] G. Bittar and G. Y. Veszely, "A general equivalent network of the input impedance of symmetric three-port circulators (short paper)," *IEEE Trans. Microw. Theory Techn.*, vol. MTT-28, no. 7, pp. 807–808, Jul. 1980, doi: [10.1109/TMTT.1980.1130171](https://doi.org/10.1109/TMTT.1980.1130171).
- [23] A. M. Hussein, M. M. Ibrahim, and S. E. Youssef, "Impedance matrix formulation of stripline circulators," *Can. Elect. Eng. J.*, vol. 5, no. 3, pp. 9–11, Jul. 1980, doi: [10.1109/CEEJ.1980.6591733](https://doi.org/10.1109/CEEJ.1980.6591733).

- [24] S. I. Shams, M. Elsaadany, and A. A. Kishk, "Including stripline modes in the Y-junction circulators: Revisiting fundamentals and key design equations," *IEEE Trans. Microw. Theory Techn.*, vol. 67, no. 1, pp. 94–107, Jan. 2019, doi: [10.1109/TMTT.2018.2880755](https://doi.org/10.1109/TMTT.2018.2880755).
- [25] T. Hao, Z. Dong, and Q. Huang, "Design of 1.9 GHz-2.6 GHz microstrip circulator based on ferrite material," in *Proc. 12th Int. Symp. Antennas, Propag. EM Theory (ISAPE)*, Hangzhou, China, Dec. 2018, pp. 1–3, doi: [10.1109/ISAPE.2018.8634221](https://doi.org/10.1109/ISAPE.2018.8634221).
- [26] J. Helszajn and W. T. Nisbet, "Circulators using planar WYE resonators," *IEEE Trans. Microw. Theory Techn.*, vol. MTT-29, no. 7, pp. 689–699, Jul. 1981, doi: [10.1109/TMTT.1981.1130430](https://doi.org/10.1109/TMTT.1981.1130430).
- [27] S. A. Ivanov, "Inherently matched Y-junction stripline circulator," *IEEE Trans. Microw. Theory Techn.*, vol. 45, no. 5, pp. 648–652, May 1997, doi: [10.1109/22.575580](https://doi.org/10.1109/22.575580).
- [28] D. M. Pozar, *Microwave Engineering*, 4th ed. Hoboken, NJ, USA: Wiley, 2011, p. 756.
- [29] *Exxelia Microwave Ferrites & FDA Y2-Series-V1.pdf*. Accessed: Mar. 28, 2022. [Online]. Available: <https://exxelia.com/fr/products/detail/622/y2-series>
- [30] S. J. Orfanidis, "A two-section dual-band Chebyshev impedance transformer," *IEEE Microw. Wireless Compon. Lett.*, vol. 13, no. 9, pp. 382–384, Sep. 2003, doi: [10.1109/LMWC.2003.817135](https://doi.org/10.1109/LMWC.2003.817135).



Vincent Olivier was born in Bergerac, France, in 1996. He received the M.S. and Ph.D. degrees in telecommunications high frequencies and optics from the University of Limoges, Limoges, France, in 2018 and 2021, respectively.

He is currently a Research and Development Engineer with Inoveos, Brive-la-Gaillarde, France. His main research interests include the design and optimization of passive filters, combiners, antennas, and gyromagnetic devices as ferrite circulators or isolators.



Thierry Monediere was born in Tulle, France, in 1964. He received the Ph.D. degree from the IRCOM Laboratory, University of Limoges, Limoges, France, in 1990.

He is currently a Professor with the Antennas and Signals Team, XLIM Research Laboratory, University of Limoges. He develops his research activities in this laboratory and works on multifunction antennas, miniature antennas, antenna arrays, and also active antennas. He also studies gyromagnetic devices as ferrite circulators or isolators.



Bertrand Lenoir was born in 1974. He received the Ph.D. degree from the University of Limoges, Limoges, France, in 2001.

He is currently the Managing Director of Inoveos, Brive-la-Gaillarde, France. His main research interests include the design and optimization of isolators, circulators, filters, couplers, and passive or active subsystems.



Hamza Turki was born in Bizerta, Tunisia, in 1991. He received the M.S. and Ph.D. degrees in telecommunications, high frequencies and optics from the University of Limoges, Limoges, France, in 2015 and 2018, respectively.

He is currently the Research and Development Manager for components at Inoveos, Brive-la-Gaillarde, France. His main research interests include gyromagnetic devices, passive filters/diplexers, couplers, and antennas.

Dr. Turki received the Best Student Paper Award at the 2018 National Conference on Material and Microwave Characterization.



Christophe Breuil was born in Brive-la-Gaillarde, France, in 1970.

He is currently the Design Manager with Inoveos, Brive-la-Gaillarde, where he is in charge of mechanical studies and manufacturing of isolators, circulators, couplers, and microwave filters. He also contributes significantly to tests and measurements of these products.



Philippe Pouliguen (Member, IEEE) received the M.S. degree in signal processing and telecommunications, the Ph.D. degree in electronics, and the "Habilitation à Diriger des Recherches" degree from the University of Rennes 1, Rennes, France, in 1986, 1990, and 2000, respectively.

In 1990, he joined the Direction Générale de l'Armement (DGA), DGA Information Superiority (DGA/IS), Bruz, France, where he was a senior expert in electromagnetic radiation and radar signatures. He was also in charge of the Expertise and ElectoMagnetism Computation (EMC) Laboratory, DGA/IS. From 2009 to 2018, he was the Head of the "acoustic and radio-electric waves" scientific domain at DGA, Paris, France. Since 2018, he has been the Innovation Manager of the "acoustic and radio-electric waves" domain at the Agence Innovation Défense (AID), Paris. His research interests include electromagnetic scattering and diffraction, radar cross section (RCS) measurement and modeling, asymptotic high-frequency methods, radar signal processing and analysis, antenna scattering problems, and electronic bandgap materials.



Laure Huitema (Member, IEEE) received the M.S. and Ph.D. degrees in telecommunications high frequencies and optics from the University of Limoges, Limoges, France, in 2008 and 2011, respectively.

From 2011 to 2012, she was a Post-Doctoral Research Fellow with the Atomic Energy Commission (CEA), Laboratory of Electronics and Information Technology (LETI), Grenoble, France. She is currently an Associate Professor with the Antennas and Signals Team within the RF systems axis, XLIM Research Institute, University of Limoges.

Her research interests include reconfigurable antennas, dielectric resonator antennas, miniature antennas, and multiband antennas and circulators. More recently, she has been working on new components for their integration inside antennas. In this framework, she is the Project Leader of an H2020 European project called MASTERS. She is currently the Director of the joint laboratory INOgyRO, which brings together the XLIM Laboratory and Inoveos.

Dr. Huitema was a recipient of the Best Student Paper Award at the 2010 IEEE International Workshop on Antenna Technology and the Best Student Paper Award at the 2010 JCMM Conference. In 2020, she won the Bronze Medal of the French National Centre for Scientific Research (CNRS).